Supporting Information

Anchored Nanocatalysts Enable Efficient Oxygen Reduction in Barium Cobaltite Cathodes

InSik Lim[a,†], Hyun Sik Yoo[b,†], DongHwan Oh[c], Gaon Heo[a], Seonmin Oh[a], Bonjae Koo[d], Wonyoung Lee[b,e,*], Jun Hyuk Kim[a,e,*]

[a] Department of Future Energy Engineering, Sungkyunkwan University, Suwon, Republic of Korea

[b] School of Mechanical Engineering, Sungkyunkwan University, Suwon, Republic of Korea

[c] Department of Chemical and Biomolecular Engineering (BK21 Four), Korea Advanced Institute of Science and Technology (KAIST), Daejeon 34141, Republic of Korea

[d] School of Chemistry and Energy, Sungshin Women's University, Seoul, Republic of Korea

[e] SKKU Institute of Energy Science and Technology (SIEST), Sungkyunkwan University, Suwon, Republic of Korea

*Corresponding authors:

Wonyoung Lee / leewy@skku.edu

Jun Hyuk Kim / jkim765@skku.edu

† These authors contributed equally.

Experimental Section

Material synthesis

Powders of $BaCo_{0.8}Ta_{0.2}O_{3-\delta}$ (BCT), $Ba_{0.95}Ag_{0.05}Co_{0.8}Ta_{0.2}O_{3-\delta}$ (BCT–Ag), $BaCo_{0.8}Ta_{0.2}O_{3-\delta}$-$Cu_{0.05}$ (BCT-Cu) and $BaCo_{0.8}Ta_{0.2}O_{3-\delta}$-$Ni_{0.05}$ (BCT–Ni) were synthesized using a conventional solid-state reaction method. Stoichiometric amounts of high purity barium carbonate ($BaCO_3$, Alfa Aesar), cobalt oxide (Co_3O_4, Sigma-Aldrich), and tantalum oxide (Ta_2O_5, Sigma-Aldrich) were mixed with dopant metal precursors (silver nitrate ($AgNO_3$, Thermo Scientific), nickel oxide (NiO, Thermo Scientific), copper oxide (CuO, Alfa Aesar)) and ball-milled in ethanol media using zirconia ball for 24 hours. The solution was then dried in an oven at 80℃ to completely evaporate the ethanol. The dried powder was pressed into pellet (green body) and calcined at 1200℃ for 10 hours. The calcined pellets were crushed using an agar mortar and subjected to a second round of ball-milling in ethanol to obtain fine powders. To ensure phase purity, the calcination and milling steps were repeated twice.

Physical characterization

The crystal structures of the synthesized powders were analyzed using X-ray diffraction (XRD, Rigaku Ultima IV) and Raman spectroscopy to confirm phase formation and structural symmetry. To determine the appropriate reduction temperature for inducing ex-solution, hydrogen temperature-programmed reduction (H_2-TPR, Micromeritics AutoChem II 2920) was performed for synthesized powders under a 10% H_2/Ar atmosphere. The morphology and distribution of ex-solved nanoparticles were examined using scanning electron microscopy (SEM, JEOL JSM-IT800). For SEM observations, 0.3 g of BCT-Ag, BCT-Cu and BCT-Ni samples were fabricated into pellet form and sintered 1150℃. The sintered pellets were then cleaved and subjected to ex-solution treatment under a 4% H_2/Ar atmosphere at 400℃ for 5

hours (BCT-Ag and BCT-Cu) and 20 hours (BCT-Ni) prior to SEM analysis. Transmission electron microscopy (TEM, Talos F200X G2) analysis was performed on the BCT-Ag, BCT-Cu, and BCT-Ni powders after ex-solution treatment under the same conditions as for SEM.

Fabrication of symmetric cells

Symmetric cells with cathode | electrolyte | cathode configuration were fabricated to evaluate the area-specific resistance (ASR) of the cathodes. Commercial Sm-doped $CeO_{2-\delta}$ (SDC, 20% Sm) powder (Fuelcellmaterials, Inc.) was used as the electrolyte. The SDC electrolyte pellets were prepared by uniaxial dry pressing of the powder and subsequently sintered at 1450℃ for 5 hours in ambient air. The synthesized oxygen electrode powders were mixed with an ink vehicle (Fuelcellmaterials, Inc.) in a 1:1 weight ratio and ball-milled in ethanol media for 24 hours to form a homogeneous slurry. After drying at 80℃ to evaporate the ethanol, the resulting slurry was applied to both sides of the sintered SDC pellet using a screen-printing technique. The printed symmetric cells were then fired at 900℃ for 2 hours under ambient air. To apply ex-solution, symmetric cells were subsequently reduced in 4% H_2/Ar at 400℃. Silver paste was then deposited as the current collector.

Electrochemical measurements of symmetric cells

Electrochemical impedance spectroscopy (EIS) measurements of the cathode symmetric cells were conducted using a Biologic VSP-300 workstation under open-circuit voltage (OCV) conditions, with an AC frequency range of 1 MHz to 0.01 Hz, in the temperature range of 500 - 650℃. The fabricated symmetric cells were mounted inside an alumina tube, and electrical contact was made using a jig supplied by Nanoionics Co. A controlled gas

mixture of O_2 and N_2 was introduced into the tube *via* digital mass flow controllers to regulate the desired oxygen partial pressure. From the acquired impedance spectra, the data points between the two intercepts of the impedance arc on the real axis were used to determine the total electrode resistance. The impedance arcs were normalized to the area of a single electrode (0.2826 cm^2). Since the symmetric cell configuration consists of two identical cathodes, the total measured resistance corresponds to the sum of both cathodes. Therefore, the resistance value was divided by two to yield the ASR of a single cathode.

Fabrication of single cells

Ni-YSZ anode-supported single cell was fabricated. NiO powder (Kojundo Chemical), YSZ powder (Tosoh Corp.), and 5 μm pore former (poly(methyl methacrylate), (PMMA, Sunjin Beauty Science) were mixed in a weight ratio of 6:4:1. The powders were dispersed in ethanol with HypermeTM KD-6 (Croda) as a dispersant and polyvinyl butyral (PVB, Sigma-Aldrich) as a binder, followed by ball milling for 24 hours. The resulting slurry was dried completely, and the obtained Ni-YSZ composite powder was uniaxially pressed into circular substrates (~700 μm thick), then sintered at 1000℃ for 3 hours to impart sufficient structural strength. The anode functional layer (AFL) and YSZ electrolyte were deposited using a spin-coating process. The AFL slurry was prepared by dispersing NiO and YSZ powders (6:4 wt ratio)—identical to those used in the bulk anode—in ethanol, with KD-6 and ethyl cellulose (50 cps, Sam Chun) serving as the dispersant and binder, respectively. This slurry was deposited onto the surface of the anode substrate and spun at 3000 rpm for 1 minute. The same procedure was used to prepare the YSZ electrolyte slurry. The AFL and YSZ layers were coated at 3000 rpm eight and two times, respectively, and then co-sintered at 1400℃ for 3 hours.

A GDC interlayer was also deposited via spin coating. GDC powder (8 g, Rhodia) was

dispersed in 20 mL of ethanol containing ethyl cellulose (10 wt ratio relative to the powder) and ball milled for 24 hours. The resulting slurry was spin-coated onto the sintered YSZ electrolyte at 3000 rpm multiple times until a target thickness of ~2 μm was achieved. The GDC interlayer was sintered at 1200°C for 3 hours. The oxygen electrode slurry was screen-printed onto the GDC surface and fired at 900°C for 2 hours in air. To ex-solve Ag, Cu and Ni nanoparticles, the electrodes were subsequently reduced in 4% H_2/Ar at 400°C. Subsequently, CuMn foam was applied as a current collector.

Electrochemical measurements of single cells

The electrochemical performance of the single cell was evaluated through current-voltage (I-V) measurements and EIS. All measurements were performed using a potentiostat (Interface 1010E, GAMRY Inc.) over a frequency range of 0.1 to 10^6 Hz, with homemade test station. The tests were conducted within the temperature range of 500-650°C. During operation, H_2 was supplied to the fuel electrode at a flow rate of 100 sccm, while air was introduced to the oxygen electrode at a flow rate of 200 sccm. Gas flows were precisely regulated using digital mass flow controllers to maintain stable and reproducible testing conditions.

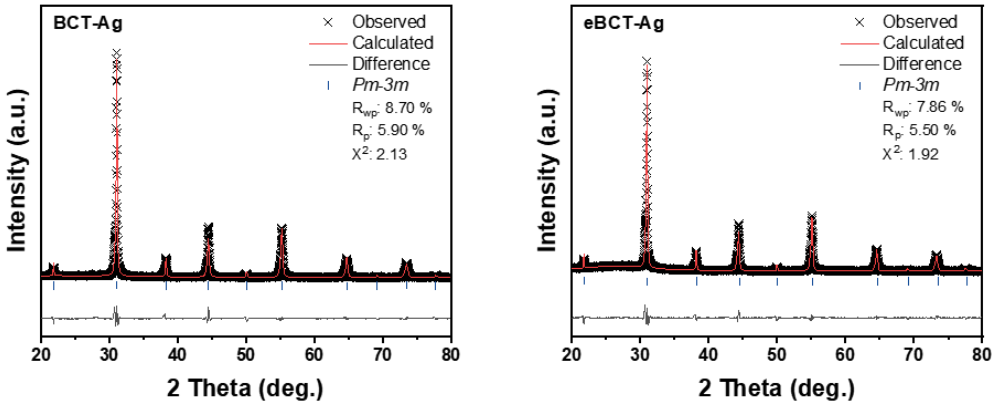

Figure S1. Rietveld refinement profiles of $BaCo_{0.8}Ta_{0.2}O_{3-\delta}$-$Ag_{0.05}$ (BCT-Ag) and ex-solved $BaCo_{0.8}Ta_{0.2}O_{3-\delta}$-$Ag_{0.05}$ (eBCT-Ag)

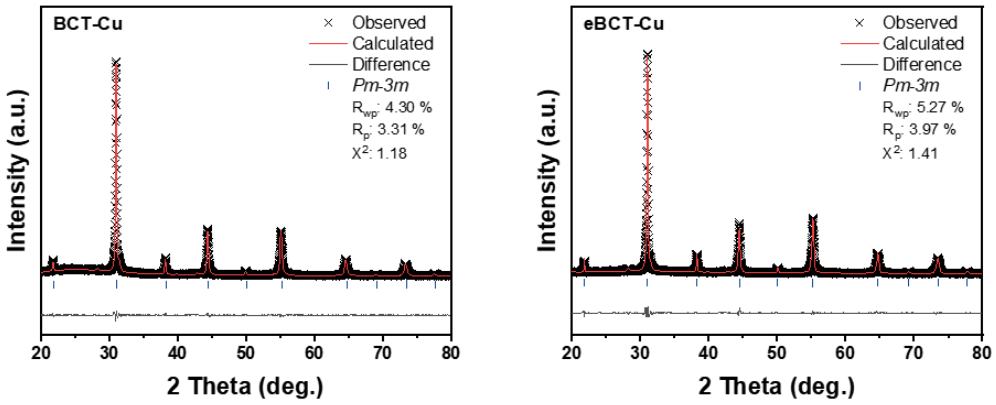

Figure S2. Rietveld refinement profiles of $Ba_{0.95}Co_{0.8}Ta_{0.2}O_{3-\delta}$-$Cu_{0.05}$ (BCT-Cu) and ex-solved $Ba_{0.95}Co_{0.8}Ta_{0.2}O_{3-\delta}$-$Cu_{0.05}$ (eBCT-Cu)

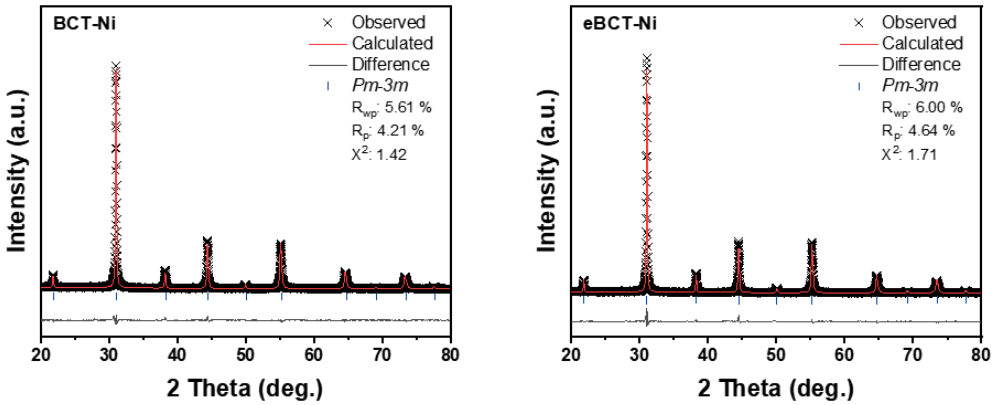

Figure S3. Rietveld refinement profiles of $Ba_{0.95}Co_{0.8}Ta_{0.2}O_{3-\delta}$-$Ni_{0.05}$ (BCT-Ni) and ex-solved $Ba_{0.95}Co_{0.8}Ta_{0.2}O_{3-\delta}$-$Ni_{0.05}$ (eBCT-Ni)

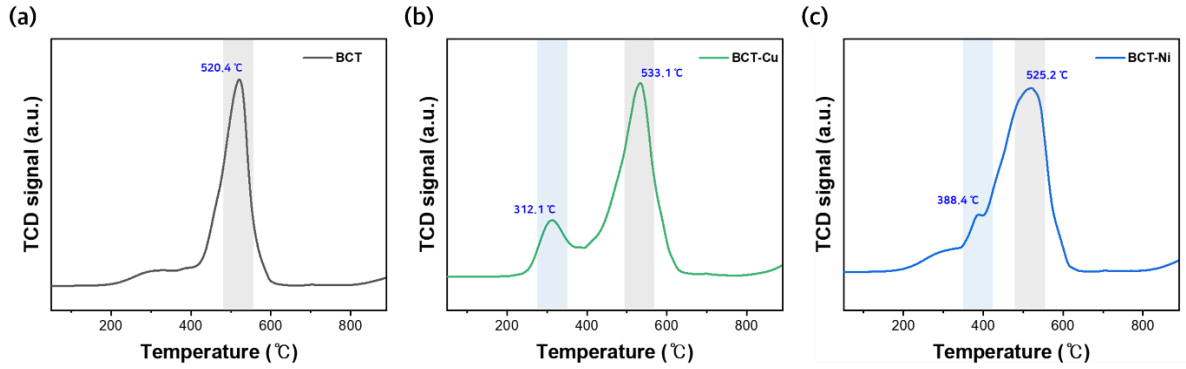

Figure S4. H_2-TPR data of (a) BCT, (b) BCT-Cu, and (c) BCT-Ni.

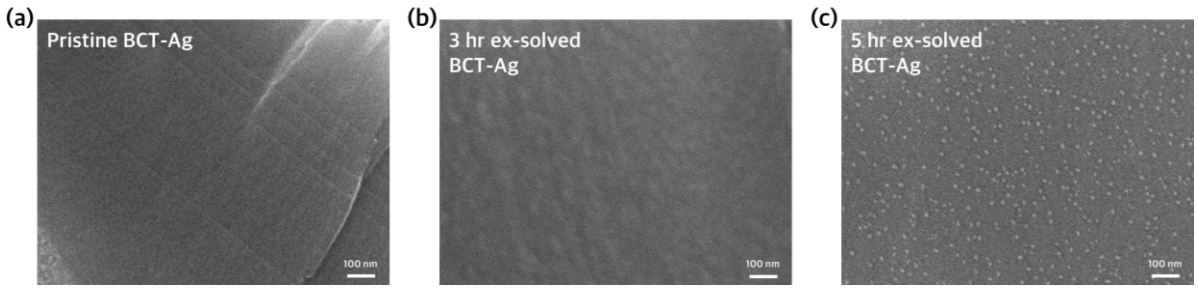

Figure S5. Time dependent morphology of ex-solved BCT-Ag after reduction in 4% H_2/Ar at 400°C: (a) 0 hr, (b) 3 hr, and (c) 5 hr.

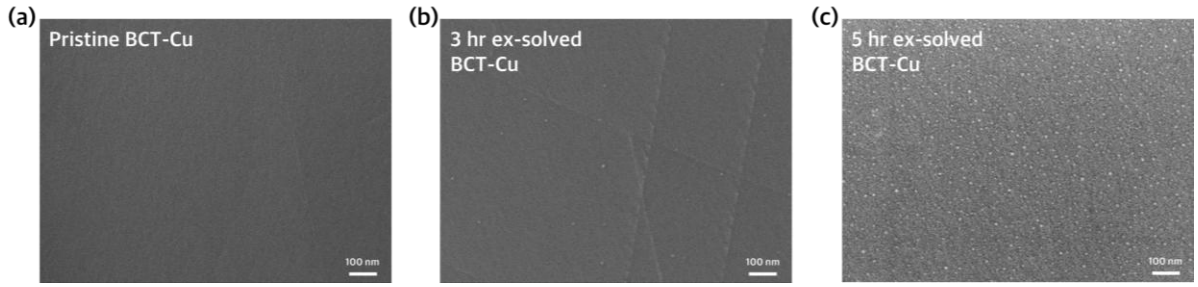

Figure S6. Time dependent morphology of ex-solved BCT-Cu after reduction in 4% H_2/Ar at 400°C: (a) 0 hr, (b) 3 hr, and (c) 5 hr.

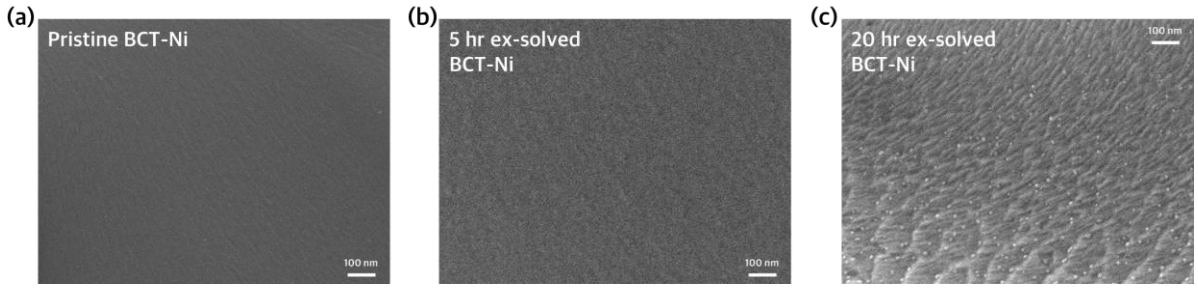

Figure S7. Time dependent morphology of ex-solved BCT-Ni after reduction in 4% H_2/Ar at 400°C: (a) 0 hr, (b) 5 hr, and (c) 20 hr.

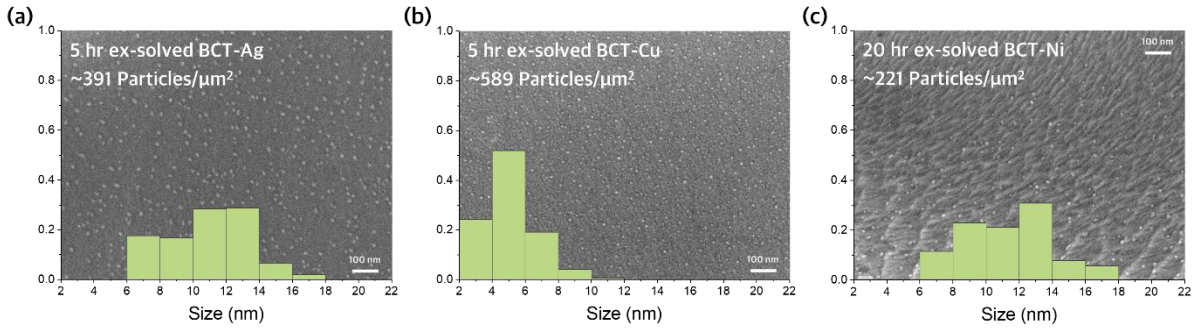

Figure S8. Nanoparticle densities observed for (a) eBCT-Ag, (b) eBCT-Cu, and (c) eBCT-Ni.

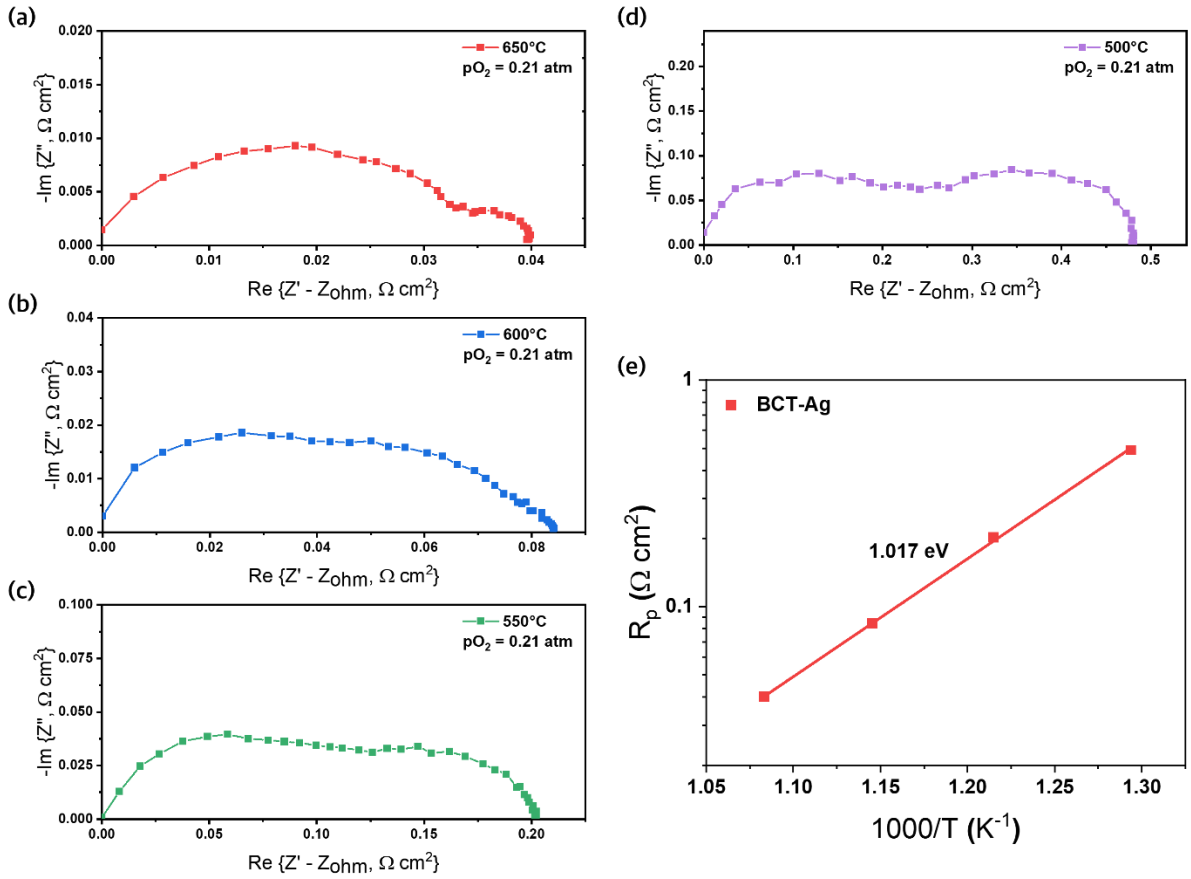

Figure S9. EIS of pristine BCT-Ag electrode with dry air at (a) 650°C, (b) 600°C, (c) 550°C, (d) 500°C. (e) Arrhenius plot of ASRs under dry air.

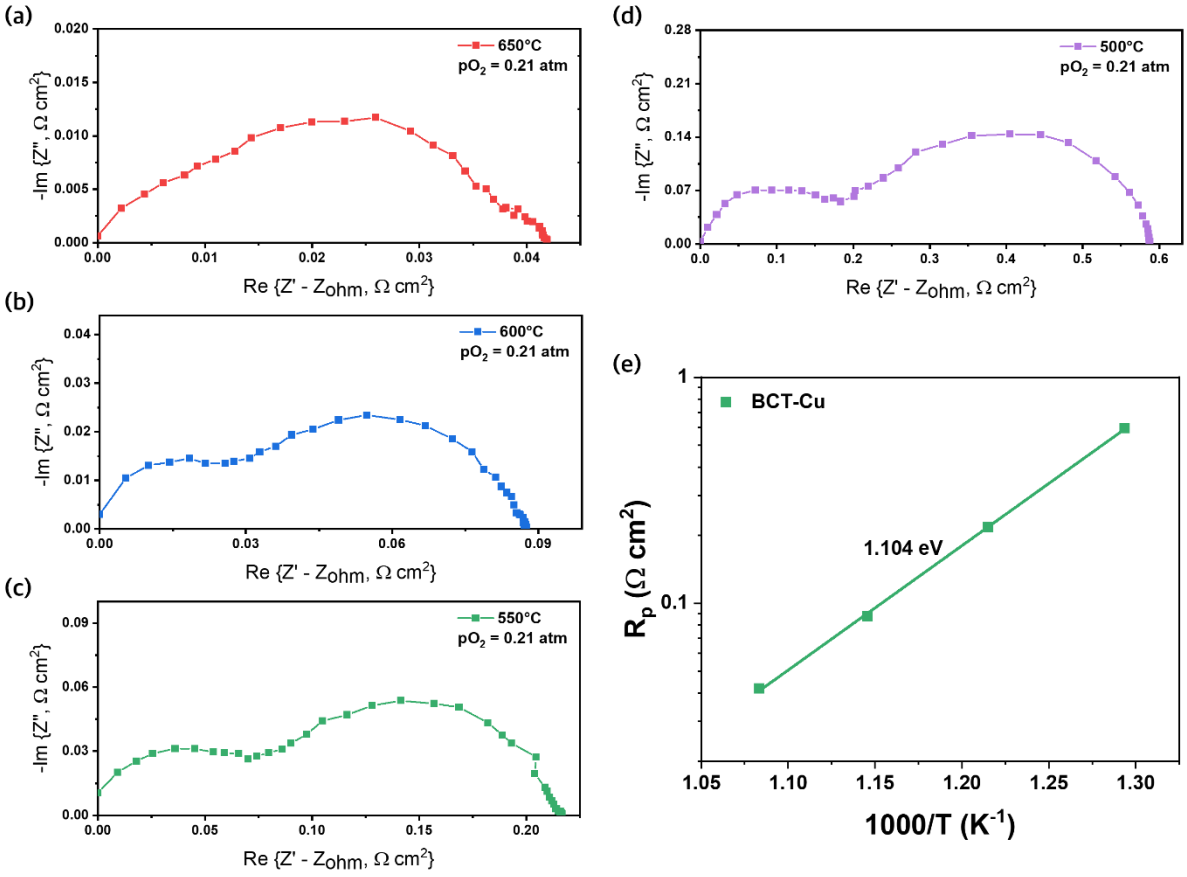

Figure S10. EIS of pristine BCT-Cu electrode with dry air at (a) 650°C, (b) 600°C, (c) 550°C, (d) 500°C. (e) Arrhenius plot of ASRs under dry air.

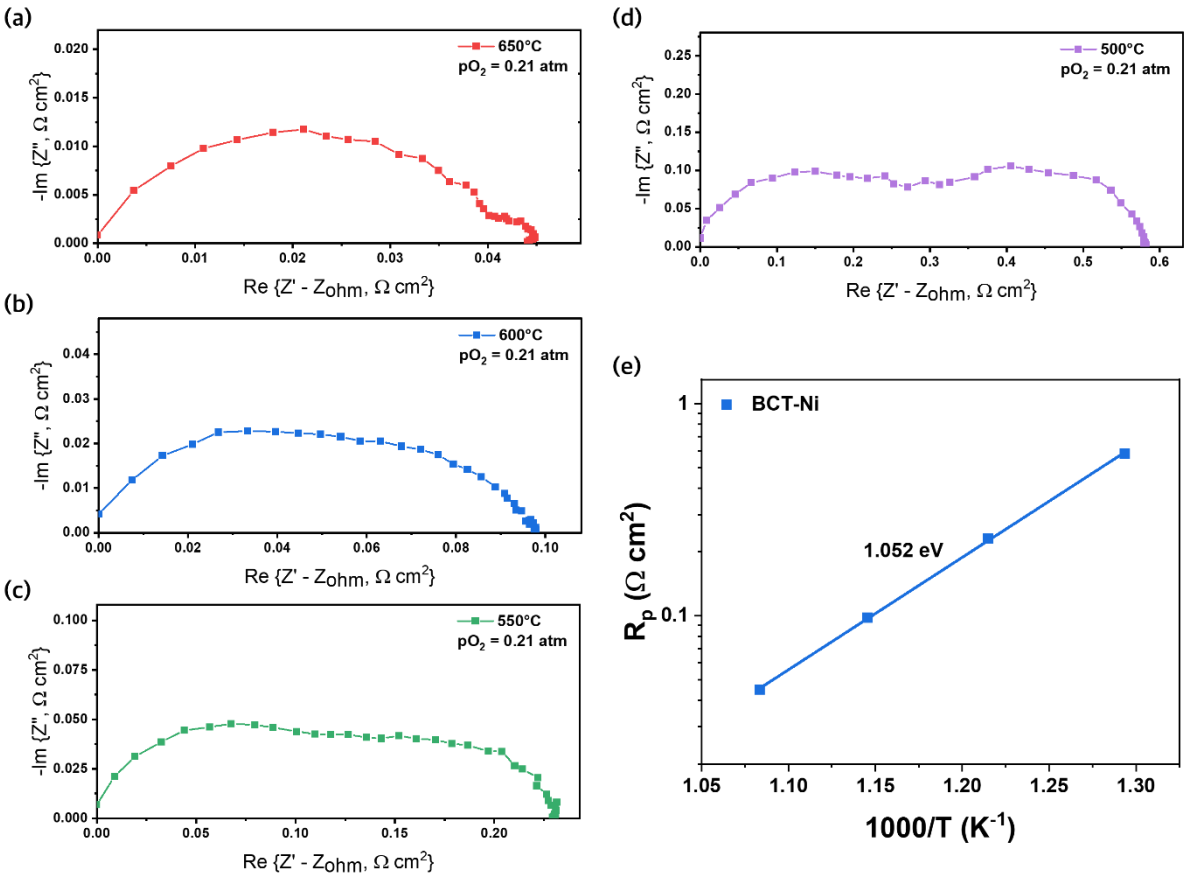

Figure S11. EIS of pristine BCT-Ni electrode with dry air at (a) 650°C, (b) 600°C, (c) 550°C, (d) 500°C. (e) Arrhenius plot of ASRs under dry air.

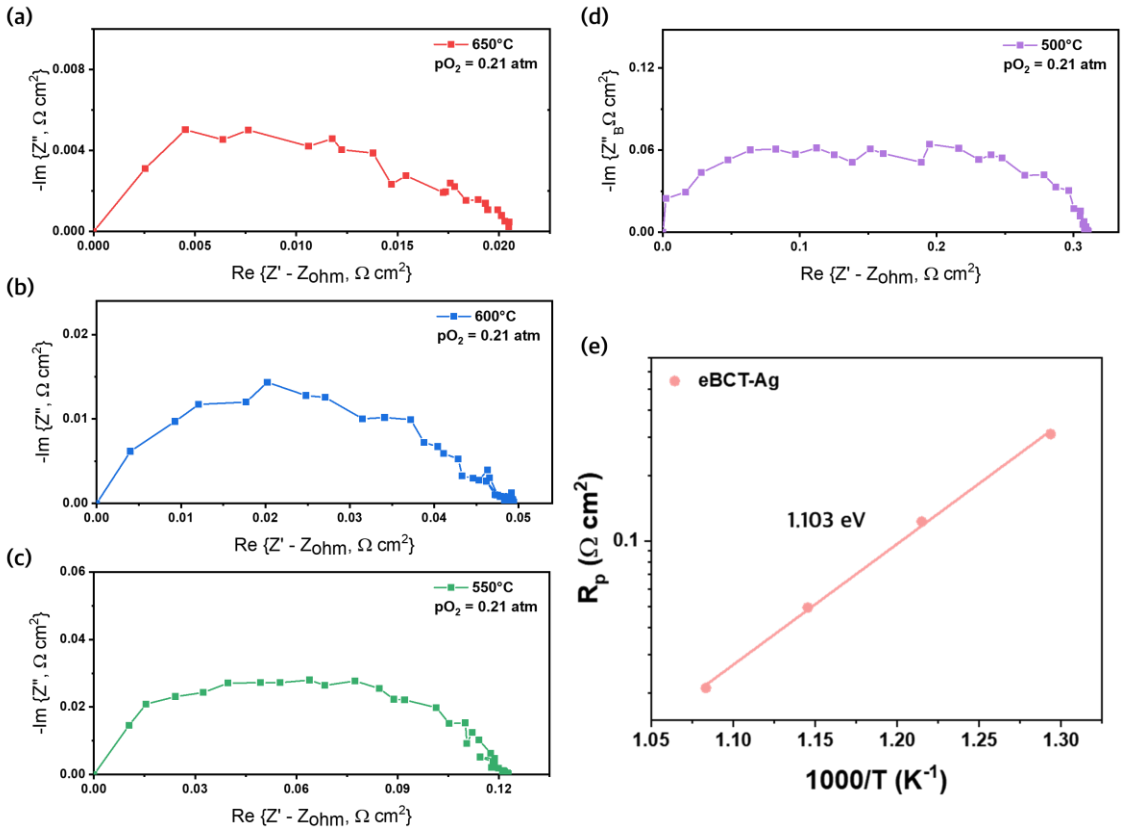

Figure S12. EIS of ex-solved BCT-Ag electrode with dry air at (a) 650°C, (b) 600°C, (c) 550°C, (d) 500°C. (e) Arrhenius plot of ASRs under dry air.

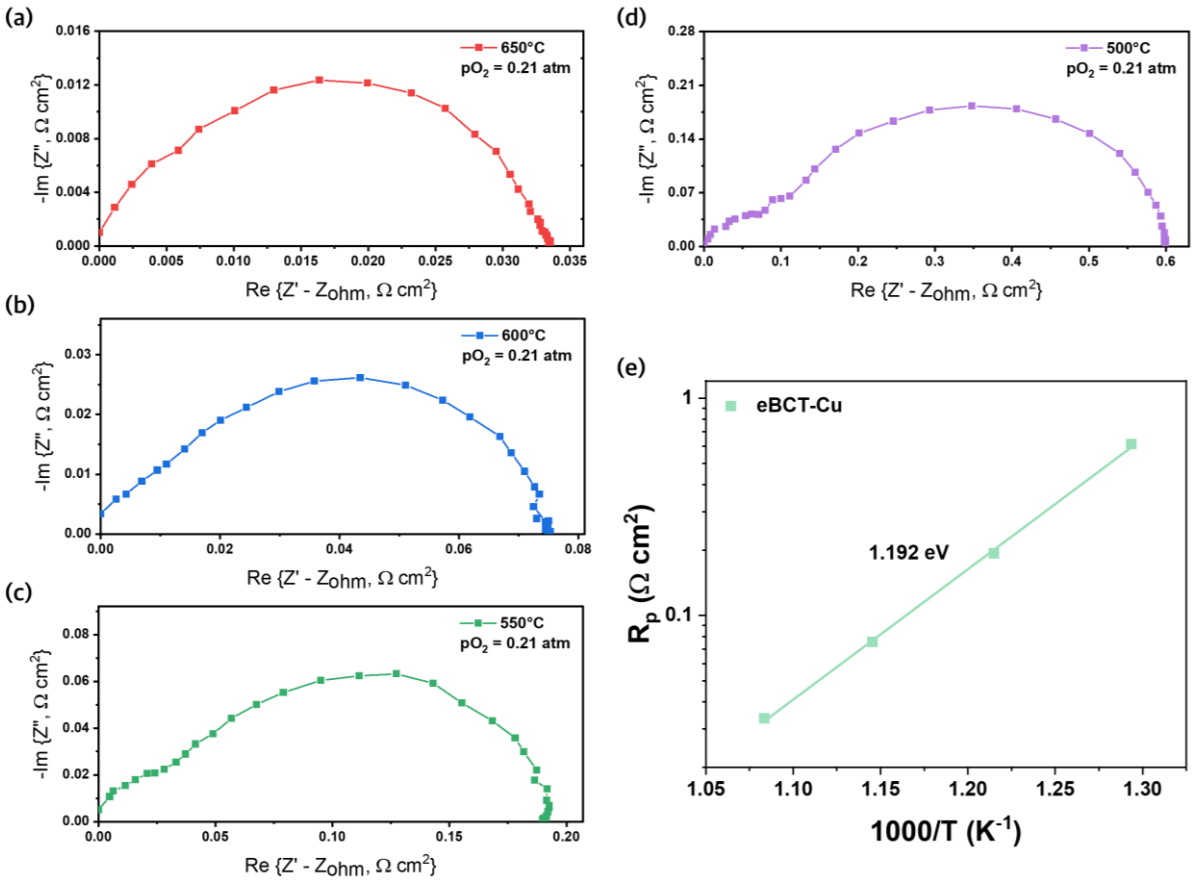

Figure S13. EIS of ex-solved BCT-Cu electrode with dry air at (a) 650°C, (b) 600°C, (c) 550°C, (d) 500°C. (e) Arrhenius plot of ASRs under dry air.

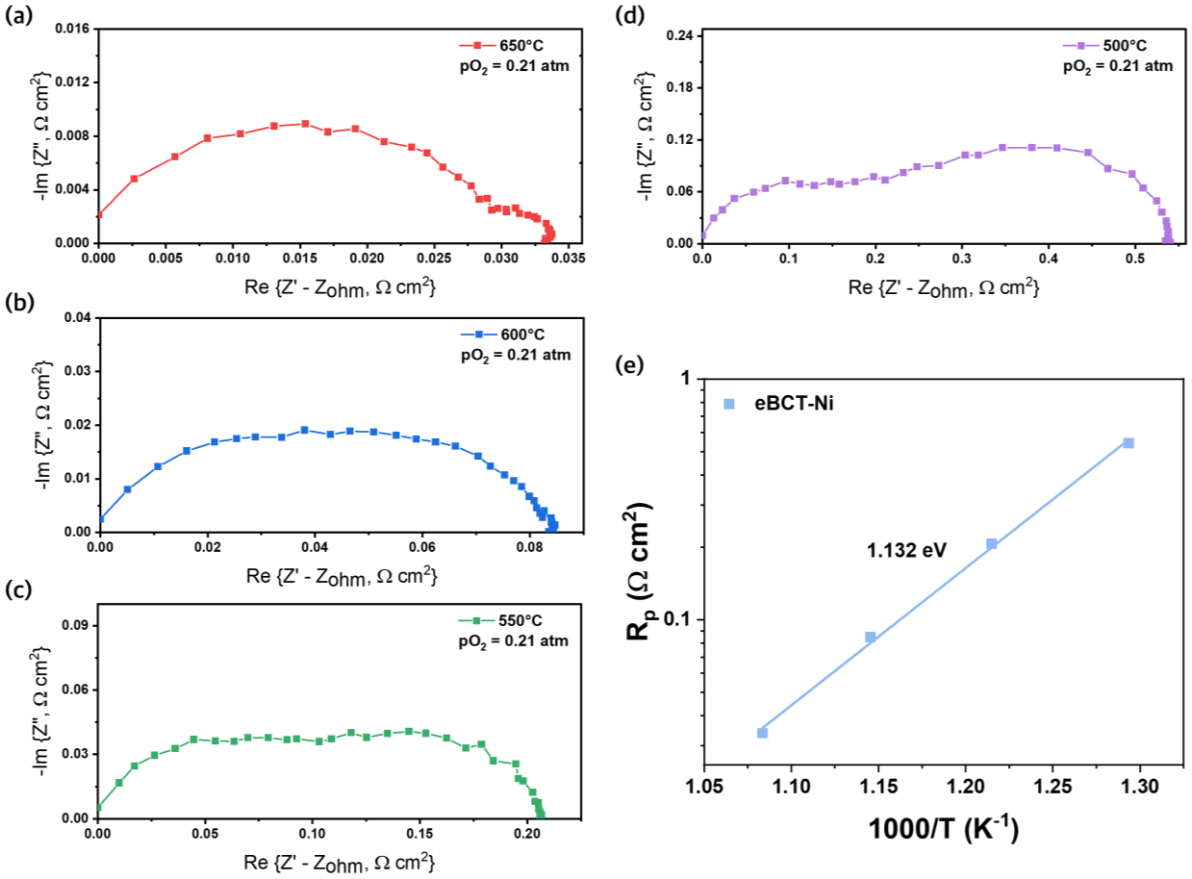

Figure S14. EIS of ex-solved BCT-Ni electrode with dry air at (a) 650°C, (b) 600°C, (c) 550°C, (d) 500°C. (e) Arrhenius plot of ASRs under dry air.

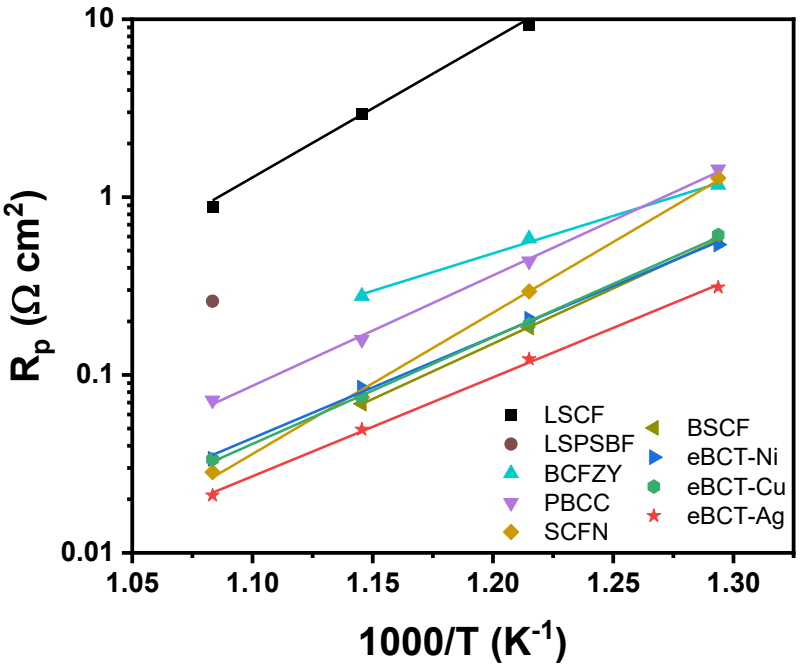

Figure S15. Performance mapping of eBCT-Ag compared with benchmark electrode materials in a symmetric cell configuration. (LSCF: $La_{0.6}Sr_{0.4}Co_{0.2}Fe_{0.8}O_{3-\delta}$,[1] LSPSBF: $(La_{0.2}Sr_{0.2}Pr_{0.2}Sm_{0.2}Ba_{0.2})FeO_{3-\delta}$,[2] BCFZY: $BaCo_{0.4}Fe_{0.4}Zr_{0.1}Y_{0.1}O_{3-\delta}$,[3] PBCC: $PrBa_{0.8}Ca_{0.2}Co_2O_{5+\delta}$,[1] SCFN: $Sr_{0.9}Ce_{0.1}Fe_{0.8}Ni_{0.2}O_{3-\delta}$,[4] BSCF: $Ba_{0.5}Sr_{0.5}Co_{0.8}Fe_{0.2}O_{3-\delta}$[5])

Cell Configuration	Polarization Resistance [Ω cm²] Temperature [°C] 500	550	600	650	Activation Energy [eV]	Reference
LSCF I SDC I LSCF	-	9.345	2.950	0.877	1.48	[1]
LSPSBF I GDC20 I LSPSBF	-	-	-	0.260	0.85	[2]
BCFZY I SDC20 I SDC	0.278	0.584	1.171	-	0.84	[3]
PBCC I SDC20 I PBCC	1.435	0.436	0.158	0.072	1.15	[1]
SCFN I SDC20 I SCFN	1.280	0.290	0.072	0.028	1.58	[4]
BSCF I SDC15 I BSCF	0.068	0.185	0.575	-	1.23	[5]
eBCT-Ni	0.540	0.206	0.085	0.034	1.13	This work
eBCT-Cu	0.613	0.192	0.075	0.033	1.19	This work
eBCT-Ag	0.311	0.123	0.049	0.021	1.10	This work

Table S1. Summary of performance metrics used for the performance map in Figure S15, comparing ex-solved electrodes with benchmark cathode materials in a symmetric cell configuration.

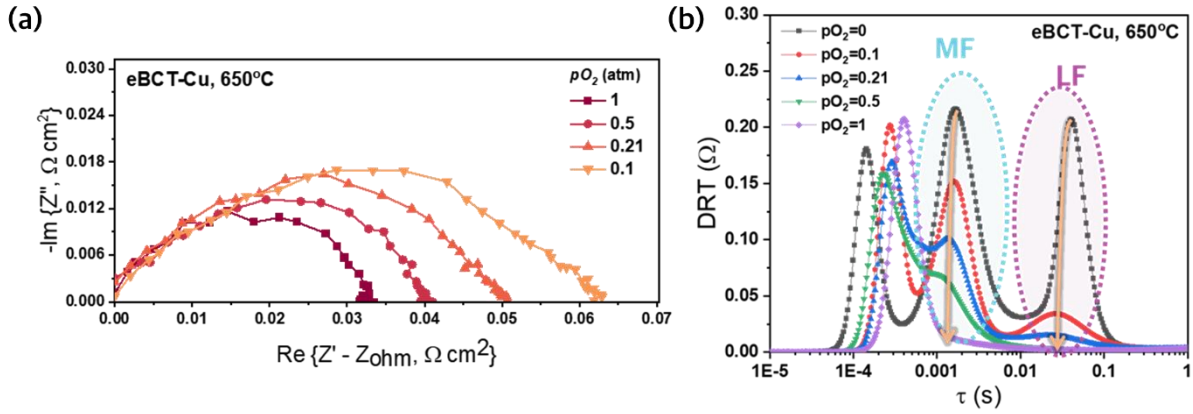

Figure S16. (a) Electrochemical impedance spectroscopy (EIS) of eBCT-Cu oxygen electrode at 650°C measured with $Sm_{0.2}Ce_{0.8}O_{2-\delta}$ (SDC) symmetric cells in dry air (pO_2 = 0.1~1 atm), and (b) corresponding distribution of relaxation time (DRT) analysis.

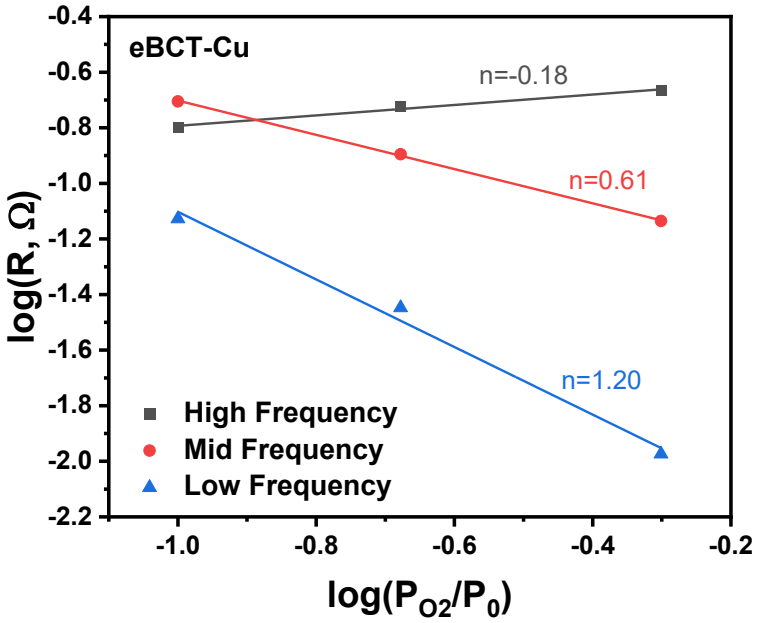

Figure S17. Oxygen partial pressure dependence of polarization resistance of eBCT-Cu.

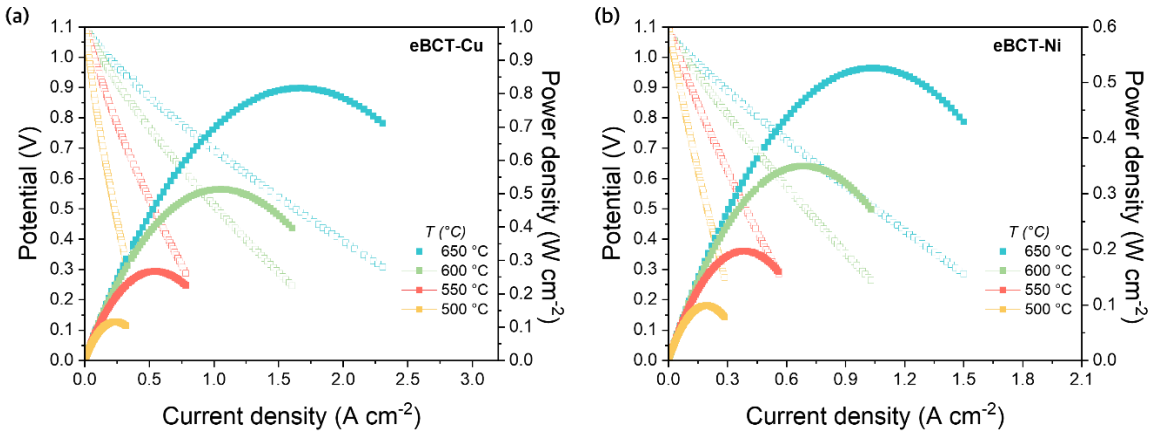

Figure S18. *I-V-P* curve of a single cell with (a) eBCT-Cu cathode, (b) eBCT-Ni electrode

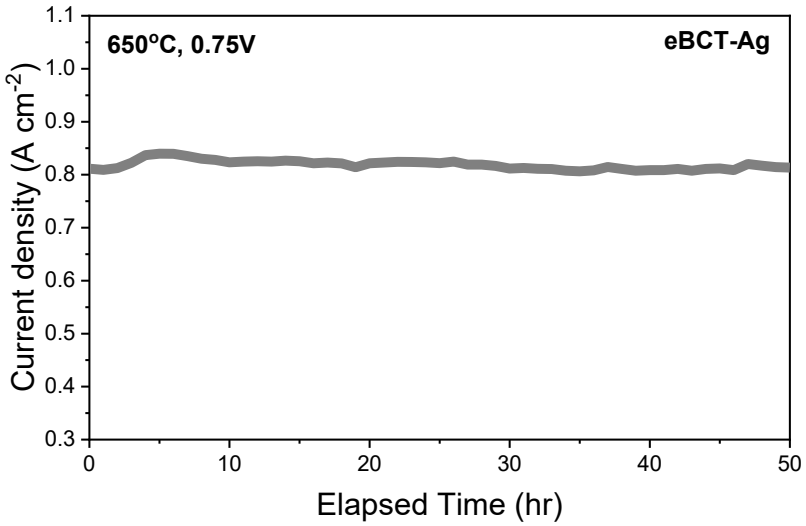

Figure S19. Short-term stability data measured with Ni-yttria-stabilized zirconia (YSZ) anode, YSZ electrolyte, $Gd_{0.1}Ce_{0.9}O_{2-\delta}$ (GDC) interlayer, and ex-solved $Ba_{0.95}Co_{0.8}Ta_{0.2}O_{3-\delta}$-$Ag_{0.05}$ (eBCT-Ag) cathode at 650°C in dry air (pO_2 = 0.21 atm).

References

1. Kim, J. H. *et al.* Promotion of oxygen reduction reaction on a double perovskite electrode by a water-induced surface modification. *Energy Environ. Sci.* **14**, 1506–1516 (2021).
2. Yao, C. *et al.* A highly active and durable iron-based high-entropy perovskite cathode for solid oxide fuel cells. *Journal of Energy Chemistry* **110**, 558–570 (2025).
3. Duan, C., Hook, D., Chen, Y., Tong, J. & O'Hayre, R. Zr and Y co-doped perovskite as a stable, high performance cathode for solid oxide fuel cells operating below 500°C. *Energy Environ. Sci.* **10**, 176–182 (2017).
4. Song, Y. *et al.* A Cobalt-Free Multi-Phase Nanocomposite as Near-Ideal Cathode of Intermediate-Temperature Solid Oxide Fuel Cells Developed by Smart Self-Assembly. *Advanced Materials* **32**, (2020).
5. Shao, Z. & Halle, S. M. A high-performance cathode for the next generation of solid-oxide fuel cells. *Nature* **431**, 170–173 (2004).